Atomic Layer-by-Layer Deposition of Pt on Pd Nanocubes for Catalysts with Enhanced Activity and Durability toward Oxygen Reduction

ARTICLE *in* NANO LETTERS · MAY 2014

Impact Factor: 13.59 · DOI: 10.1021/nl501205j · Source: PubMed

12 AUTHORS, INCLUDING:

Shuifen Xie
Xiamen University
39 PUBLICATIONS **1,213** CITATIONS
SEE PROFILE

Sang-Il Choi
Kyungpook National University
33 PUBLICATIONS **609** CITATIONS
SEE PROFILE

Ning Lu
Chinese Academy of Agricultural Sciences
162 PUBLICATIONS **2,079** CITATIONS
SEE PROFILE

Lei Zhang
Georgia Institute of Technology
21 PUBLICATIONS **471** CITATIONS
SEE PROFILE

NANO LETTERS

Letter

pubs.acs.org/NanoLett

Atomic Layer-by-Layer Deposition of Pt on Pd Nanocubes for Catalysts with Enhanced Activity and Durability toward Oxygen Reduction

Shuifen Xie,[†,‡] Sang-Il Choi,[†] Ning Lu,[§] Luke T. Roling,[∥] Jeffrey A. Herron,[∥] Lei Zhang,[†,‡] Jinho Park,[⊥] Jinguo Wang,[§] Moon J. Kim,[§] Zhaoxiong Xie,[‡] Manos Mavrikakis,[∥] and Younan Xia*[,†,⊥]

[†]The Wallace H. Coulter Department of Biomedical Engineering, Georgia Institute of Technology and Emory University, Atlanta, Georgia 30332, United States

[‡]State Key Laboratory of Physical Chemistry of Solid Surfaces and Department of Chemistry, College of Chemistry and Chemical Engineering, Xiamen University, Xiamen, Fujian 361005, China

[§]Department of Materials Science and Engineering, University of Texas at Dallas, Richardson, Texas 75080, United States

[∥]Department of Chemical and Biological Engineering, University of Wisconsin-Madison, Madison, Wisconsin 53706, United States

[⊥]School of Chemistry and Biochemistry, Georgia Institute of Technology, Atlanta, Georgia 30332, United States

Supporting Information

ABSTRACT: An effective strategy for reducing the Pt content while retaining the activity of a Pt-based catalyst is to deposit the Pt atoms as ultrathin skins of only a few atomic layers thick on nanoscale substrates made of another metal. During deposition, however, the Pt atoms often take an island growth mode because of a strong bonding between Pt atoms. Here we report a versatile route to the conformal deposition of Pt as uniform, ultrathin shells on Pd nanocubes in a solution phase. The introduction of the Pt precursor at a relatively slow rate and high temperature allowed the deposited Pt atoms to spread across the entire surface of a Pd nanocube to generate a uniform shell. The thickness of the Pt shell could be controlled from one to six atomic layers by varying the amount of Pt precursor added into the system. Compared to a commercial Pt/C catalyst, the Pd@Pt_{nL} (n = 1−6) core−shell nanocubes showed enhancements in specific activity and durability toward the oxygen reduction reaction (ORR). Density functional theory (DFT) calculations on model (100) surfaces suggest that the enhancement in specific activity can be attributed to the weakening of OH binding through ligand and strain effects, which, in turn, increases the rate of OH hydrogenation. A volcano-type relationship between the ORR specific activity and the number of Pt atomic layers was derived, in good agreement with the experimental results. Both theoretical and experimental studies indicate that the ORR specific activity was maximized for the catalysts based on Pd@Pt_{2-3L} nanocubes. Because of the reduction in Pt content used and the enhancement in specific activity, the Pd@Pt_{1L} nanocubes showed a Pt mass activity with almost three-fold enhancement relative to the Pt/C catalyst.

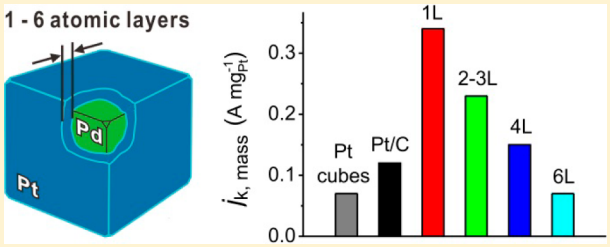

KEYWORDS: *Platinum-based catalyst, bimetallic catalyst, oxygen reduction reaction, fuel cell, core−shell nanostructure*

Platinum is a key component of many industrial catalysts, including those currently used in the catalytic converters, as well as those for petroleum reforming and nitric acid production.[1−3] It is also the catalyst of choice for the oxygen reduction reaction (ORR) occurring on the cathode of a proton-exchange membrane fuel cell (PEMFC).[4−6] As one of the scarcest noble metals on Earth, however, its availability has become a major concern for all existing and emerging applications built upon Pt catalysts. To increase the utilization efficiency and thereby reduce the Pt content in a catalyst, a number of methods have been explored to improve the specific and mass activities of Pt-based catalysts.[7−10] Among them, the most promising approach is to deposit Pt atoms as ultrathin skins of only a few atomic layers on nanoparticles made of a more abundant and/or less expensive metal.[11,12]

For single-crystal substrates, one can generate ultrathin coatings of Pt with well-controlled thicknesses using vacuum deposition, followed by annealing at a very high temperature (≥1000 °C).[13] This technique, however, cannot be extended to substrates with nanometer sizes and suspended in liquid media. In recent years, a displacement method involving under-potentially deposited (UPD) Cu was developed to generate monolayers or sub-monolayers of Pt on nanoparticles made of Pd or other metals (as well as their alloys with Pt).[14,15] These core−shell nanostructures were shown to possess enhanced mass activity toward the ORR. In addition, ultrathin skins of Pt

Received: April 1, 2014
Revised: May 1, 2014

   dx.doi.org/10.1021/nl501205j | *Nano Lett.* XXXX, XXX, XXX−XXX

were formed on the surfaces of nanocrystals made of Pt_3Ni, Pt_3Co, or PtCu through annealing and/or dealloying to obtain ORR catalysts with enhanced performance.[9,16,17] While these prior studies have demonstrated the feasibility to generate advanced electrocatalysts based on ultrathin skins of Pt, it has been extremely difficult (or impossible) to precisely and reliably control the thicknesses of the Pt overlayers down to the atomic scale.

Since Pt and Pd are very similar in terms of lattice constant and chemical reactivity, they can be readily prepared as bimetallic core−shell nanocrystals with a single-crystal structure and good stability via epitaxial, conformal deposition.[10] The current cost of Pd is only half of that of Pt, making Pd a good candidate for the core to help reduce the material cost of a catalyst. In addition, both theoretical and experimental studies have shown that a combination of Pd and Pt can lower the surface electronic d-band center of Pt to bring in enhancement for certain catalytic reactions, such as the ORR.[10,18−21] Meanwhile, the use of Pd can prevent Pt from corrosion by sacrificing Pd or up-shifting the dissolution potential of Pt and thus help improve the catalytic durability.[10,22] Although great strides have been made in the synthesis of Pd@Pt core−shell nanocrystals, direct deposition of Pt overlayers on Pd nanocrystals with a precise control over the number of Pt atomic layers has been met with limited success. For example, traditional atomic layer deposition (ALD) in a gas phase and most of the solution-phase methods often generate Pt overlayers with a polycrystalline structure and uneven thickness.[23,24] The intrinsic high surface free energy and interatomic bond energy (307 kJ/mol) of Pt tend to direct the deposition of Pt toward an island growth mode (Volmer−Weber mode).[25,26] We hypothesize that the conditions used in all of the previously reported solution-phase methods were too mild to provide an adequate thermochemical energy needed to break the strong Pt−Pt bonds. As a result, the deposited Pt atoms favored island growth rather than layer-by-layer epitaxy on the surface of the nanoscale substrates. In addition, the capping agents adsorbed on the nanoscale substrate tend to prevent Pt atoms from spreading across the entire surface of a substrate, resulting in the localized nucleation and growth of Pt only from certain regions of the substrate.[27,28]

Here, we introduce a solution-phase method for the conformal deposition of ultrathin shells of Pt on Pd nanocrystals with control on the atomic scale. In a proof-of-concept experiment, Pd nanocubes were used as suspended nanoscale substrates (or seeds) for the deposition of Pt atoms in a layer-by-layer fashion. The success of our approach relies on the relatively slow injection of a Pt precursor at a sufficiently high temperature to allow Pt atoms to spread across the entire surface of a Pd seed from the initially deposited sites to generate Pd@Pt_{nL} core−shell nanocubes. The number (n) of Pt atomic layers on each Pd cubic seed could be precisely controlled from a monolayer to multiple layers by simply adjusting the amount of Pt precursor introduced into the reaction solution. Our ORR measurements indicate that catalysts based on the Pd@Pt_{nL} (n = 1−4) core−shell nanocubes exhibited enhancements in specific and mass activities relative to a commercial Pt/C catalyst. To understand the correlation between the ORR specific activity and the number of Pt atomic layers, we also performed periodic, self-consistent density functional theory (DFT) calculations by adopting a slab model of a Pd(100) surface with n (n = 1−5) atomic layers of Pt being deposited pseudomorphically on the top, denoted as Pt_{nL}*/Pd(100). The ORR mechanistic analysis on this model system gave a volcano-shaped plot for the ORR specific activity as a function of the number of Pt atomic layers, which was in nearly quantitative agreement with the experimental data obtained for the Pd@Pt_{nL} core−shell nanocubes.

The Pd cubic seeds had an average edge length of 18 nm, as shown by the transmission electron microscopy (TEM) image and the corresponding size distribution (Figure S1). Some of them were slightly elongated along one of the directions, but their surfaces were still covered by {100} facets. For simplicity, they are collectively called "nanocubes" in our discussion. We used a solution of $Na_2PtCl_6·6H_2O$ in ethylene glycol (EG) as the precursor to Pt atoms. With the use of a syringe pump, the Pt precursor was slowly injected at a rate of 4.0 mL/h into another EG solution that contained Br^- ions as a capping agent for the {100} facets,[28] ascorbic acid (AA) as a reducing agent (in addition to EG) for the Pt precursor, and poly(vinylpyrrolidone) (PVP) as a colloidal stabilizer, respectively. The synthesis had to be conducted at a temperature as high as 200 °C to increase the reduction power of EG and promote surface diffusion for the deposited Pt atoms. Once a drop of the precursor was introduced into the reaction solution, the Pt^{IV} species should be immediately reduced to Pt atoms and then deposited onto the surfaces of the Pd cubic seeds. As a result, the concentration of the Pt atoms in the reaction solution could be kept at a low level to effectively prevent self-nucleation for the newly generated Pt atoms, allowing us to obtain Pd@Pt_{nL} core−shell nanocubes with tightly controlled numbers of Pt atomic layers.

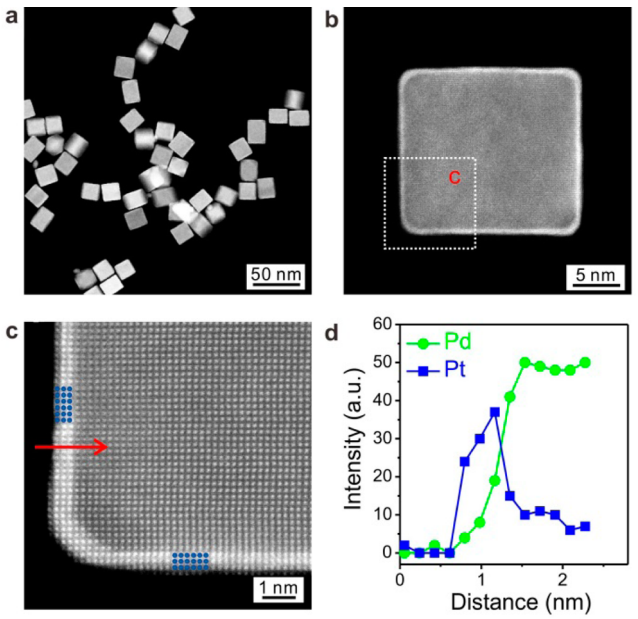

Figure 1. Structural and compositional analyses of the Pd@$Pt_{2−3L}$ core−shell nanocubes. (a) Low-magnification HAADF-STEM image showing the cubic shape and good uniformity of the sample; (b) high-magnification HAADF-STEM image of an individual particle showing that the surface of the Pd cubic seed was evenly coated with an ultrathin shell of Pt (with a brighter contrast); (c) atomic-resolution HAADF-STEM image taken from the corner region marked by boxes in (b), showing that the number of Pt atomic layers was around 3; (d) elemental distribution by the EDX line scan analysis along the red arrow in (c).

dx.doi.org/10.1021/nl501205j | Nano Lett. XXXX, XXX, XXX−XXX

Table 1. Average Number (n) of Pt Atomic Layers Calculated from the ICP-MS Data for the Pd and Pt Contents in the Pd@Pt_{nL} Samples, the Weight Percentage (wt %) of Pt Derived from the n of Pt Atomic Layers and the Size of Pd Nanocubes, and the wt % of Pt Calculated from the ICP-MS Data for Pd and Pt Contents

sample	n of Pt atomic layers	wt % of Pt calculated from the value of n	wt % of Pt calculated from the ICP-MS data
Pd@Pt_{1L}	1	10.9	11.6
Pd@Pt_{2-3L}	2–3	19.9 (2L) 27.6 (3L)	23.1
Pd@Pt_{4L}	4	34.2	33.9
Pd@Pt_{6L}	6	44.8	44.0

Figure 1 shows electron microscopy characterizations of the Pd@Pt_{nL} nanocubes obtained by adding 7.0 mL of the Pt precursor solution. During the deposition of Pt atomic layers, the cubic shape of the Pd seeds was retained, together with their flat and smooth surfaces (Figure 1, a and b), implying the involvement of layer-by-layer growth. Figure 1b shows an aberration-corrected high-angle annular dark-field scanning TEM (HAADF-STEM) image taken from an individual Pd@Pt_{nL} nanocube. There was a good contrast between the Pt shell and the Pd core because of the difference in atomic number between these two elements. The core–shell nanocubes had an average edge length of 19.2 nm (Figure S2), which was 1.2 nm greater than that of the initial Pd cubic seeds. On average, the thickness of the Pt shell deposited on each Pd(100) face was around 0.6 nm. From the enlarged atomic-resolution HAADF-STEM image shown in Figure 1c, the number of Pt atomic layers was estimated to be 3. Based on the unit cell parameters of Pt, three atomic layers correspond to a thickness of 0.59 nm (Figure S3), which is in good agreement with the value of 0.6 nm measured from the change to average edge length. We also quantitatively analyzed the average number (n) of Pt atomic layers for the Pd@Pt_{nL} nanocubes by inductively coupled plasma mass spectrometry (ICP-MS). Since ICP-MS averages over a much larger number of particles than electron microscopy, the number of Pt atomic layers is referred to the ICP-MS data in the following discussion. As shown in Table 1, the average number of Pt atomic layers was 2–3 for this sample, so it is denoted as Pd@Pt_{2-3L}. Figure 1d shows a line profile of energy-dispersive X-ray spectroscopy (EDX) analysis recorded along the red line marked in Figure 1c, further confirming the elemental compositions for the Pt shell and Pd core.

Since the Pt precursor was slowly injected into the reaction solution, the resultant Pt atoms should only go through heterogeneous nucleation on the Pd seeds. As such, it was feasible to control the thickness of the Pt shells with atomic precision by controlling the amount of Pt precursor added into the reaction solution. As demonstrated in Figure 2, the number of Pt atomic layers could be changed to 6, 4, and 1 (Table 1) by

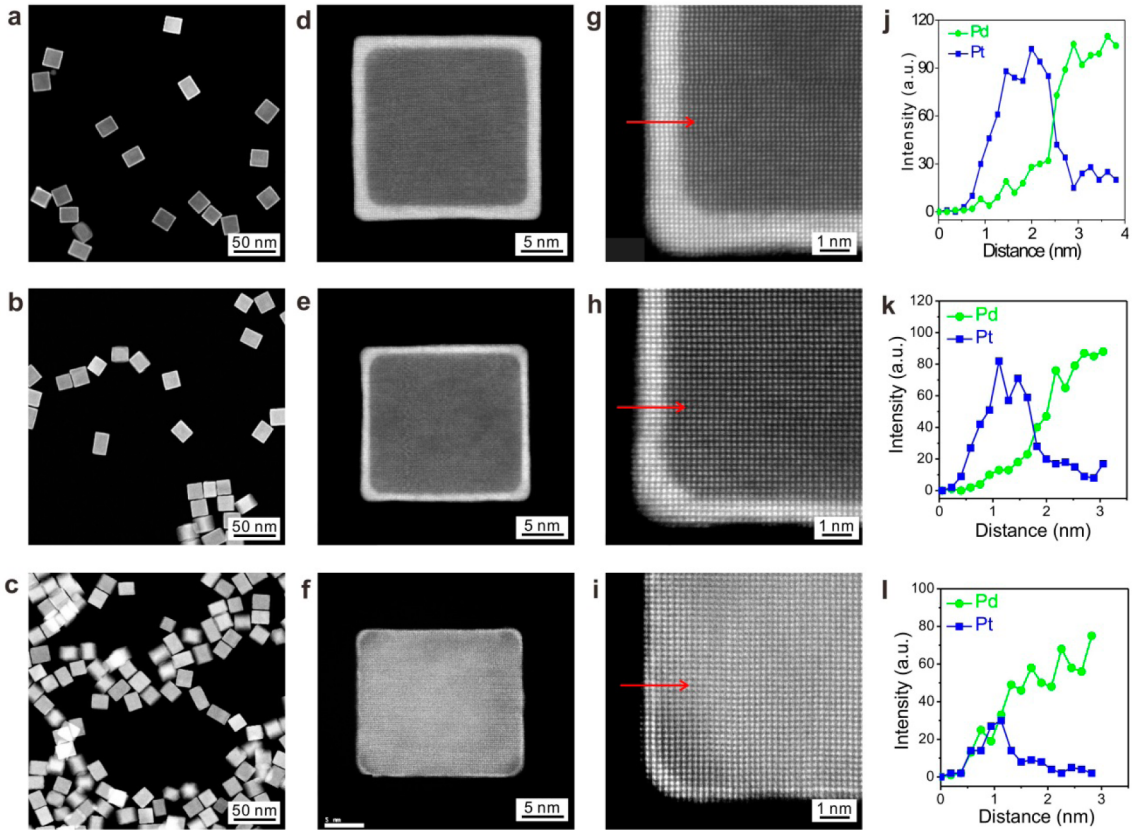

Figure 2. Controlling the number of Pt atomic layers. (a–c) Low-magnification HAADF-STEM images showing a large number of (a) Pd@Pt_{6L}, (b) Pd@Pt_{4L}, and (c) Pd@Pt_{1L} nanocubes; (d–f) HAADF-STEM images of individual (d) Pd@Pt_{6L}, (e) Pd@Pt_{4L}, and (f) Pd@Pt_{1L} nanocubes; (g–i) atomic-resolution HAADF-STEM images taken from the (g) Pd@Pt_{6L}, (h) Pd@Pt_{4L}, and (i) Pd@Pt_{1L} nanocubes, revealing the numbers of Pt atomic layers; (j–l) EDX line scan analyses of the (j) Pd@Pt_{6L}, (k) Pd@Pt_{4L}, and (l) Pd@Pt_{1L} nanocubes along the red arrows marked in (g–i).

dx.doi.org/10.1021/nl501205j | Nano Lett. XXXX, XXX, XXX–XXX

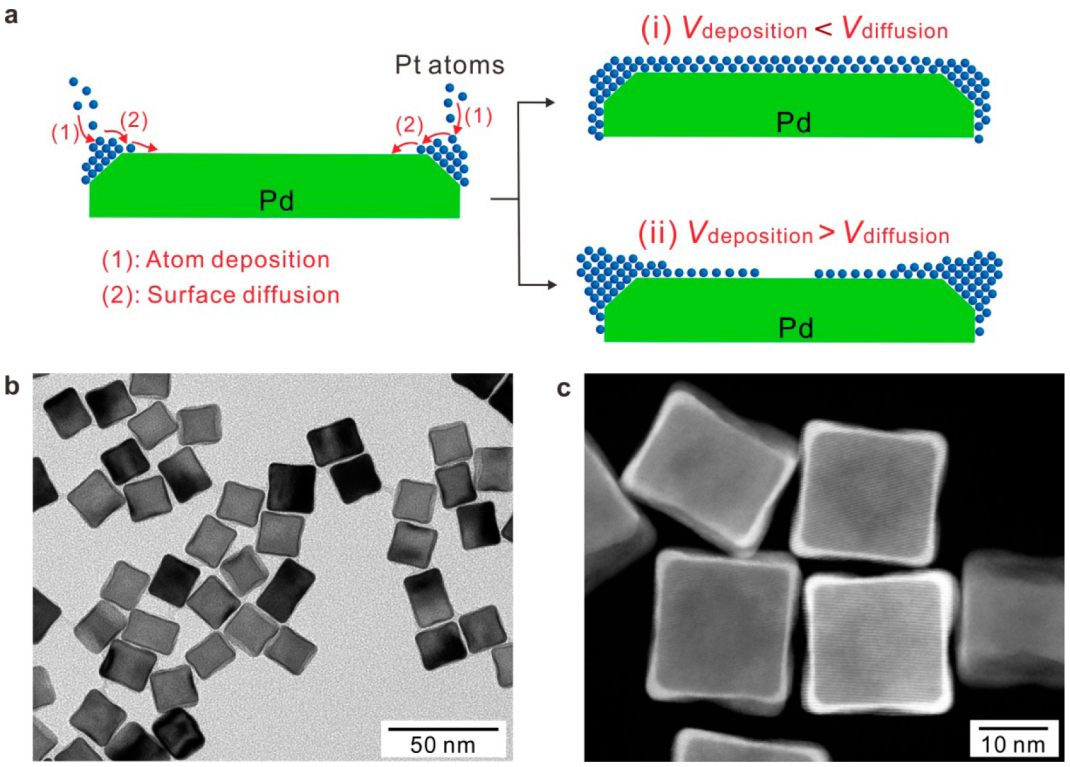

Figure 3. Mechanistic study of the deposition of Pt atoms on Pd nanocubes. (a) A schematic illustration showing the deposition of Pt atoms on Pd cubic seeds, which could be divided into two major steps: (1) deposition of Pt atoms at the corner sites and (2) surface diffusion of the deposited Pt atoms from the corners to side faces. When $V_{deposition} < V_{diffusion}$ (case (i), the Pt atoms can evenly spread on the entire Pd{100} faces, generating Pd@Pt_{nL} core−shell nanocubes with well-controlled number of Pt atomic layers. When $V_{deposition} > V_{diffusion}$ (case (ii), most of the deposited Pt atoms will stay at the corner sites, generating Pd−Pt concave nanocubes. (b, c) TEM image and HAADF-STEM image of the Pd−Pt concave nanocubes synthesized using the standard procedure at a faster injection rate (40 mL/h) for the precursor. The added volume of $Na_2PtCl_6·6H_2O$ solution (0.25 mg/mL) was 19.0 mL.

altering the volume of the Pt precursor solution from 7.0 mL to 19.0, 12.0, and 3.0 mL, respectively. The samples shown in Figure 2, a−c, correspond to Pd@Pt_{6L}, Pd@Pt_{4L}, and Pd@Pt_{1L} nanocubes. The core−shell structures containing different numbers of Pt atomic layers were also confirmed by HAADF-STEM images (Figure 2, d−i) and EDX line-scan profiles (Figure 2, j−l). These results clearly demonstrate that we could readily manipulate the thickness of the Pt shells from a single atomic layer to multiple layers. The EDX line scan for the Pt_{1L} nanocubes (Figure 2l) suggests that the surface composition of these nanocubes might contain a mixture of Pt and Pd atoms. To understand this phenomenon, we derived the thermodynamically most favorable surface termination for Pd@Pt_{1L} nanocubes using DFT (GGA-PW91) calculations on model (100) slabs (see Figure S4 and Supporting Information for details). Our results suggest that, under vacuum, the system would be most stable if the surface was terminated by Pd, together with a full monolayer of Pt in the first subsurface layer. However, in the presence of O or OH, a mixed Pd−Pt termination was preferred (Figure S5).

As illustrated in Figure 3a, the Pt atoms were initially deposited at the corners of a Pd cubic seed because the Pd{100} side faces were blocked by the chemisorbed Br^- ions.[27] The deposited Pt atoms could then diffuse from the corners to the edges and side faces in the following steps.[28] As a result, the morphology of the final products was largely determined by the difference in rates responsible for Pt atom deposition ($V_{deposition}$) and surface diffusion ($V_{diffusion}$). A flat surface could be achieved for the Pt overlayer on the side face of a Pd cubic seed through a combination of slow injection for the Pt precursor (and thus small $V_{deposition}$) and high reaction temperature (and thus large $V_{diffusion}$). To be more specific, when the deposition of Pt atoms was slower than surface diffusion ($V_{deposition} < V_{diffusion}$), the Pt atoms could be evenly spread across the Pd(100) side face, generating a Pd@Pt_{nL} core−shell nanocube with well-controlled numbers of Pt atomic layers. In contrast, when the injection rate for the Pt precursor was increased (and thus large $V_{deposition}$, Figure 3, b and c) or when the reaction temperature was reduced to 140 °C (and thus small $V_{diffusion}$, Figure S6), the morphology of the products was switched to concave nanocubes. In this case, the deposition of Pt atoms was faster than surface diffusion ($V_{deposition} > V_{diffusion}$), and most of the deposited Pt atoms would stay at the corner sites due to inadequate surface diffusion.

We benchmarked the ORR activities of the as-obtained Pd@Pt_{nL} nanocubes against a commercial Pt/C catalyst (20 wt % 3.2 nm Pt particles supported on Vulcan XC-72 carbon, Premetek Co.) and Pt nanocubes (9 nm in edge length).[29] The Pd@Pt_{nL} nanocubes were loaded on carbon supports (Pd@Pt_{nL}/C, Figure S7) and then heated in acetic acid at 60 °C for 12 h to clean the surface before they were deposited on rotating disk electrodes (RDEs) made of glassy carbon. The cyclic voltammograms (CVs) of all of the catalysts (Figure S8a) were recorded at room temperature in N_2-saturated 0.1 M $HClO_4$ solutions at a sweeping rate of 50 mV/s in the potential range of 0.08−1.1 V versus reversible hydrogen electrode (RHE). Figure S9 shows the specific electrochemical active surface areas

dx.doi.org/10.1021/nl501205j | Nano Lett. XXXX, XXX, XXX−XXX

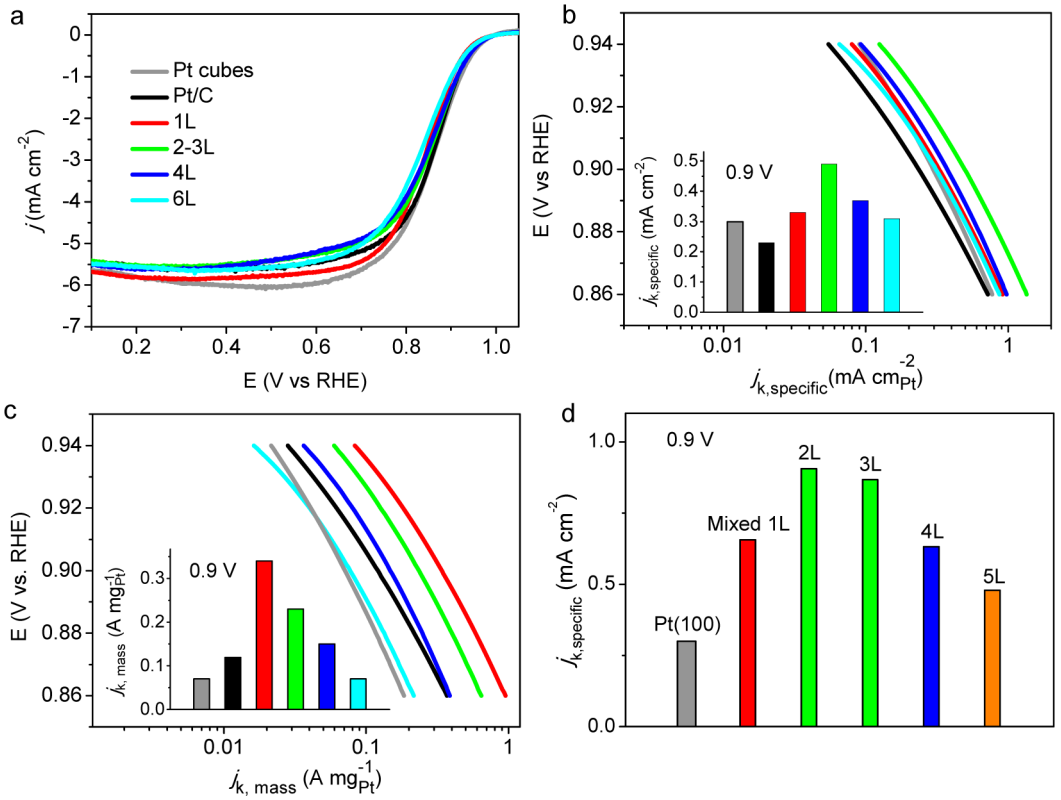

Figure 4. Benchmarking the electrocatalytic properties of the Pd@Pt_{nL}/C catalysts against a commercial Pt/C catalyst and Pt nanocubes of 9 nm in edge length. (a) ORR polarization curves for the catalysts at room temperature in O_2-saturated 0.1 M aqueous $HClO_4$ solutions. The current density of each catalyst was normalized to the geometric area of RDE (0.196 cm^2). (b) Specific and (c) mass ORR activities given as kinetic current densities (j_k) normalized to the ECSA and Pt loading of the catalyst, respectively. (d) ORR specific activities calculated for the Pt_{nL}*/Pd(100) model. The specific activities were normalized to that of Pt(100), for which the experimental activity was taken to be the same as the calculated activity. The bar for "mixed 1L" corresponds to the Pd@Pt_{1L} core−shell nanocubes measured experimentally. The bars for "2L" and "3L" correspond to the Pd@Pt_{2-3L} core−shell nanocubes measured experimentally. The bar for "5L" was not tested experimentally.

(ECSAs) derived from the charges responsible for the H_{upd} desorption between 0.08 and 0.45 V (Figure S8b) and normalized to the Pt mass. Because of its high dispersion of Pt atoms, the specific ECSA of the Pd@Pt_{1L}/C (104.1 m^2/g_{Pt}) was almost twice that of the Pt/C catalyst (51.4 m^2/g_{Pt}) and four times that of the Pt nanocubes (23.9 m^2/g_{Pt}). As the average number of Pt atomic layers was increased, the specific ECSAs gradually dropped to 47.6, 39.7, and 24.9 m^2/g_{Pt} for the Pd@Pt_{2-3L}/C, Pd@Pt_{4L}/C, and Pd@Pt_{6L}/C catalysts, respectively. It should be pointed out that the ECSAs of these Pd@Pt_{nL}/C catalysts were all comparable to those of the Pt/C and Pt nanocubes even though their sizes (18−21.2 nm) were much larger than those of Pt/C (3.2 nm) and Pt nanocubes (9 nm). The large specific ECSAs associated with the Pd@Pt_{nL}/C (n < 4) catalysts suggest an increase in utilization efficiency for the Pt atoms when these core−shell cubes are used as electrocatalysts.

The ORR activity was measured in an O_2-saturated 0.1 M aqueous $HClO_4$ solution at room temperature with a metal (including both Pd and Pt) loading of 30.6 $\mu g/cm^2$ on a RDE for each catalyst. Figure 4a shows the positive-going ORR polarization curves. To achieve a better understanding of the surface and mass effects, we calculated the kinetic currents from the ORR polarization curves by following the Koutecky−Levich equation[30] and then normalized the kinetic current to the ECSA ($j_{k,specific}$) and Pt mass ($j_{k,mass}$), respectively. As illustrated in Figure 4b, the specific activities of Pd@Pt_{nL}/C ($n \leq 4$) catalysts were all enhanced in the potential region between 0.86 and 0.94 V relative to the state-of-the-art Pt/C catalyst and Pt nanocubes. It should be pointed out that the ORR activity of the Pt(100) surface in a non-adsorbing electrolyte such as $HClO_4$ is lower than those of other low-index facets such as (111) and (110).[16,31] Therefore, the enhanced specific activity for the Pd@Pt_{nL}/C catalysts should be attributed to the strain arising from the mismatch in lattice constant between Pd and Pt and the ligand effect reflecting the electronic coupling between the two metals.[18,20,21,35,36] A combination of the ligand effect and compressive lateral strain can lower the Pt d-band center, weakening the binding of OH_{ad} species on the Pt(100) surface. At 0.9 V, the $j_{k,specific}$ values of the four different Pd@Pt_{nL}/C (n = 1, 2−3, 4, and 6) catalysts also showed a volcano-shaped dependence on the number of Pt atomic layers, with a maximum point corresponding to Pd@Pt_{2-3L}/C, which was 1.6 times that of the Pt nanocubes (inset of Figure 4b). Deposition of more than three atomic layers of Pt on the Pd nanocubes tends to weaken the ligand effect, which is then screened by Pt electrons, leading to an increase in the binding strength of OH_{ads} and a concomitant reduction in specific activity.

To better understand the experimentally observed volcano-type relationships between the ORR specific activity and the number of Pt atomic layers (insets of Figure 4b), we performed self-consistent periodic DFT calculations (GGA-PW91, see Supporting Information for details). We first calculated the binding energies of O and OH on Pt(100), as a model for the Pt nanocubes, and Pt_{nL}*/Pd(100), as a model for the Pd nanocubes covered by n-layers of Pt atoms (Table S1). Our

dx.doi.org/10.1021/nl501205j | Nano Lett. XXXX, XXX, XXX−XXX

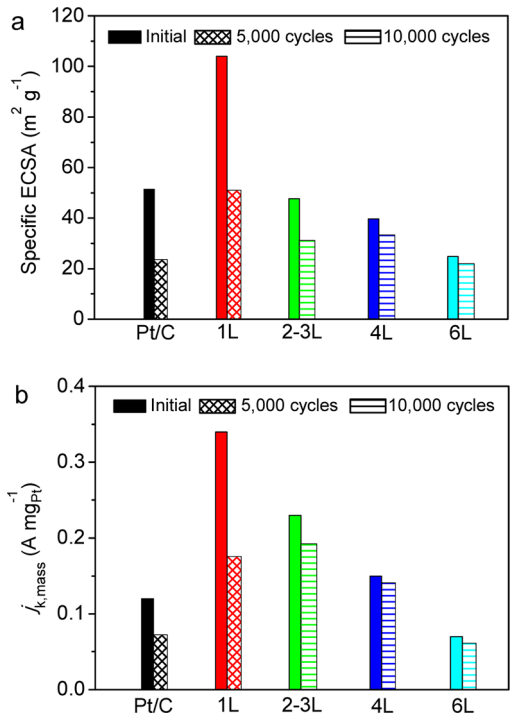

Figure 5. Durability tests of the ORR electrocatalysts. A comparison of (a) ECSAs and (b) mass activities given as kinetic current densities (j_k) at 0.9 V (vs. RHE) for the Pt/C and Pd@Pt$_{nL}$/C catalysts before and after accelerated ORR durability tests. The durability tests were carried out at room temperature in an O_2-saturated 0.1 M aqueous $HClO_4$ solution with the cyclic potential sweeping between 0.6 and 1.1 V at a rate of 0.1 V/s.

total energy calculations suggest that, in the presence of O or OH, a mixed Pd−Pt termination is preferred for Pd@Pt$_{1L}$, which is in line with the EDX mapping shown in Figure 2l. From the binding energies calculated, using a simple electrochemical model,[32] we obtained the reaction energetics (ΔG) for O and OH hydrogenation at 0.9 V (Table S2). We found that the rate-determining step on these surfaces is OH hydrogenation. Therefore, we would expect the Pd@Pt$_{nL}$ nanocubes to have higher ORR activity if their OH binding energies were weaker than that of the Pt nanocubes. Through a combination of ligand[33−35] and strain[34−36] effects, the binding of OH to these Pt$_{nL}$*/Pd(100) surfaces was very mildly modulated with respect to Pt(100) but sufficiently enough to markedly improve the ORR specific activity compared to that of Pt(100). To better compare these theoretical predictions with the experimentally observed relative activities, we calculated the activity for OH hydrogenation on these surfaces, referenced to that on Pt(100). Due to the exponential dependence on the reaction energetics, even small modulations of the binding energy of OH can significantly affect ORR activity. Similar to the experimental data, we obtained a volcano-type trend for the specific activity (at 0.9 V) as a function of the number of Pt atomic layers (Figure 4d and Table S3). In the plot, the specific activities were normalized to that of the Pt(100) surface, which was assumed to take the experimental value. The theoretical bar for "mixed 1L" corresponds to the experimentally measured Pd@Pt$_{1L}$ core−shell nanocubes (see Supporting Information). A maximum specific activity was predicted for the system with two Pt atomic layers, suggesting that the Pd@Pt$_{2-3L}$ nanocubes should have the highest ORR specific activity among all of the catalysts tested.

An important indicator for the commercialization potential of Pt-based catalysts is their mass activities. As shown in Figure 4c, the catalysts based on Pd@Pt$_{nL}$ nanocubes with 1−4 atomic layers of Pt all showed substantially improved mass activities relative to the state-of-the-art Pt/C catalyst. The overall enhancements in Pt mass activity can be attributed to (i) improvement in specific activity and (ii) changes in Pt dispersion. The specific activity follows a volcano trend, maximizing at 2−3 Pt atomic layers. However, the specific ECSA decreases with each additional layer of Pt atoms. Balancing these two effects, the Pt mass activity was maximized with only one layer of Pt atoms. The mass activity of Pd@Pt$_{1L}$/C at 0.9 V was almost three times that of the commercial Pt/C catalyst.

We also evaluated the long-term stability of the Pd@Pt$_{nL}$/C catalysts through accelerated durability tests by applying linear potential sweeps between 0.6 and 1.1 at 0.1 V/s in an O_2-saturated 0.1 M $HClO_4$ solution at room temperature. Previous studies indicate that the small particles in commercial Pt/C were barely retained under the harsh condition of an ORR durability test due to the high proportions of low-coordination atoms on the surfaces.[19,37] Compared to the commercial Pt/C catalyst, the durability was greatly improved for all the Pd@Pt$_{nL}$/C catalysts based on the specific ECSAs and mass ORR activities given as kinetic current densities (j_k) at 0.9 V (Figure 5). For example, the specific ECSAs of Pd@Pt$_{2-3L}$/C, Pd@Pt$_{4L}$/C, and Pd@Pt$_{6L}$/C were reduced by 35%, 16%, and 12% after 10 000 cycles. Although the sizes of the Pd@Pt$_{nL}$ cubes were around 20 nm, it is worth pointing out that their specific ECSAs after the tests were still comparable to or even higher than that of the Pt/C catalyst after 5000 cycles (Figure 5a). At 0.9 V, the Pd@Pt$_{4L}$/C only showed a 6% loss in mass activity after 10 000 cycles, while the losses for the Pd@Pt$_{1L}$/C and the Pt/C catalysts were 48% and 40% after 5000 cycles, respectively (Figure 5b). The increased durability for the catalysts with thicker Pt overlayers can be attributed to better passivation of the Pd cores by the Pt shells, as confirmed by TEM analysis. For both the Pd@Pt$_{1L}$/C and Pd@Pt$_{2-3L}$/C catalysts, most of the Pd cores were dissolved during the durability tests. The remaining Pt atoms migrated to the corners and edges to generate Pt cubic frames. In contrast, very few of the Pd cores were dissolved during the durability test for the Pd@Pt$_{6L}$/C catalysts. These results suggest a new strategy for generating Pt-based catalysts with excellent performance by depositing Pt atoms as ultrathin shells on Pd nanocrystals with relatively large sizes (e.g., >10 nm). The mass activity could be retained and even enhanced by dispersing essentially all Pt atoms on the surface. By moving away from nanoparticles of only a few nanometers in size (like those in the commercial Pt/C catalyst), the durability could also be greatly improved.

In summary, this work demonstrates that the surface of a Pd nanocube could be coated with a conformal, ultrathin shell of Pt with thickness precisely controllable down to the atomic scale by using a slow injection rate for the Pt precursor and a reaction temperature at 200 °C. The Pd@Pt$_{nL}$ core−shell nanocubes with well-controlled shell thicknesses showed enhanced catalytic activity and durability toward ORR as compared to the state-of-the-art Pt/C catalyst and Pt nanocubes. In particular, the Pd@Pt$_{2-3L}$ nanocubes showed the highest specific activity toward ORR among all of the Pd@

dx.doi.org/10.1021/nl501205j | Nano Lett. XXXX, XXX, XXX−XXX

Pt_{nL} catalysts tested, which is also rationalized by our DFT-based mechanistic analysis.

■ ASSOCIATED CONTENT

Supporting Information

Experimental details, method for DFT calculations, TEM images, and CVs of the catalysts. This material is available free of charge via the Internet at http://pubs.acs.org.

■ AUTHOR INFORMATION

Corresponding Author

*E-mail: younan.xia@bme.gatech.edu (Y.X.).

Author Contributions

S.X. and S.-I.C. contributed equally.

Author Contributions

S.X. conducted the syntheses, collected and analyzed the data, and wrote the paper. S.-I.C. carried out the electrochemical measurements, analyzed the data, and wrote the paper. N.L, J.W., and M.J.K. carried out the aberration-corrected TEM characterizations. L.R., J.H., and M.M. performed the DFT modeling and analysis and contributed to the preparation of manuscript. L.Z. and Z.X. were involved in the data analysis and discussion. J.P. did the ICP-MS measurements. Y.X. conceived the experiments, supervised the study, analyzed the data, and wrote the paper.

Notes

The authors declare no competing financial interest.

■ ACKNOWLEDGMENTS

This work was supported in part by start-up funds from the Georgia Institute of Technology and a grant from DOE (BES, Office of Chemical Sciences, grant DE-FG02-05ER15731). As jointly supervised PhD students from Xiamen University, S.X. and L.Z. were also partially supported by Fellowships from the China Scholarship Council. Computations were performed at supercomputing centers located at EMSL, which is sponsored by the DOE Office of Biological and Environmental Research at PNNL; CNM at ANL, supported by DOE contract DE-AC02-06CH11357; and NERSC, supported by DOE contract DE-AC02-05CH11231.

■ REFERENCES

(1) Ertl, G.; Knözinger, H.; Schüth, F.; Weitkamp, J. *Handbook of Heterogeneous Catalysis*, 2nd ed.; Wiley-VCH: Weinheim, 2008.
(2) Balaj, O. P.; Balteanu, I.; Roßteuscher, T. T. J.; Beyer, M. K.; Bondybey, V. E. *Angew. Chem., Int. Ed.* **2004**, *43*, 6519−6522.
(3) Chen, A.; Holt-Hindle, P. *Chem. Rev.* **2010**, *110*, 3767−3804.
(4) Steele, B. C. H.; Heinzel, A. *Nature* **2001**, *414*, 345−352.
(5) Guo, S.; Zhang, S.; Sun, S. *Angew. Chem., Int. Ed.* **2013**, *52*, 8526−8544.
(6) Debe, M. K. *Nature* **2012**, *486*, 43−51.
(7) Tsung, C.-K.; Kuhn, J. N.; Huang, W.; Aliaga, C.; Hung, L.-I.; Somorjai, G. A.; Yang, P. *J. Am. Chem. Soc.* **2009**, *131*, 5816−5822.
(8) Tian, N.; Zhou, Z.-Y.; Sun, S.-G.; Ding, Y.; Wang, Z. L. *Science* **2007**, *316*, 732−735.
(9) Stamenkovic, V. R.; Mun, B. S.; Arenz, M.; Mayrhofer, K. J. J.; Lucas, C. A.; Wang, G.; Ross, P. N.; Markovic, N. M. *Nat. Mater.* **2007**, *6*, 241−247.
(10) Zhang, H.; Jin, M.; Xia, Y. *Chem. Soc. Rev.* **2012**, *41*, 8035−8049.
(11) Liu, Y.; Gokcen, D.; Bertocci, U.; Moffat, T. P. *Science* **2012**, *338*, 1327−1330.
(12) Gao, C.; Lu, Z.; Liu, Y.; Zhang, Q.; Chi, M.; Cheng, Q.; Yin, Y. *Angew. Chem., Int. Ed.* **2012**, *51*, 5629−5633.
(13) Toyoda, E.; Jinnouchi, R.; Ohsuna, T.; Hatanaka, T.; Aizawa, T.; Otani, S.; Kido, Y.; Morimoto, Y. *Angew. Chem., Int. Ed.* **2013**, *52*, 4137−4140.
(14) Brankovic, S. R.; Wang, J. X.; Adzic, R. R. *Surf. Sci.* **2001**, *474*, L173−L179.
(15) Adzic, R. R.; Zhang, J.; Sasaki, K.; Vukmirovic, M. B.; Shao, M.; Wang, J. X.; Nilekar, A. U.; Mavrikakis, M.; Valerio, J. A.; Uribe, F. *Top. Catal* **2007**, *46*, 249−262.
(16) Stamenkovic, V. R.; Fowler, B.; Mun, B. S.; Wang, G.; Ross, P. N.; Lucas, C. A.; Markovic, N. M. *Science* **2007**, *315*, 493−497.
(17) Strasser, P.; Koh, S.; Anniyev, T.; Greeley, J.; More, K.; Yu, C.; Liu, Z.; Kaya, S.; Nordlund, D.; Ogasawara, H.; Toney, M. F.; Nilsson, A. *Nat. Chem.* **2010**, *2*, 454−460.
(18) Kitchin, J. R.; Nørskov, J. K.; Barteau, M. A.; Chen, J. G. *Phys. Rev. Lett.* **2004**, *93*, 156801.
(19) Lim, B.; Jiang, M.; Camargo, P. H. C.; Cho, E. C.; Tao, J.; Lu, X.; Zhu, Y.; Xia, Y. *Science* **2009**, *324*, 1302−1305.
(20) Wang, J. X.; Inada, H.; Wu, L.; Zhu, Y.; Choi, Y.; Liu, P.; Zhou, W.-P.; Adzic, R. R. *J. Am. Chem. Soc.* **2009**, *131*, 17298−17302.
(21) Wang, X.; Orikasa, Y.; Takesue, Y.; Inoue, H.; Nakamura, M.; Minato, T.; Hoshi, N.; Uchimoto, Y. *J. Am. Chem. Soc.* **2013**, *135*, 5938−5941.
(22) Greeley, J.; Nørskov, J. K. *Electrochim. Acta* **2007**, *52*, 5829−5836.
(23) Aaltonen, T.; Ritala, M.; Sajavaara, T.; Keinonen, J.; Leskelä, M. *Chem. Mater.* **2003**, *15*, 1924−1928.
(24) Mackus, A. J. M.; Verheijen, M. A.; Leick, N.; Bol, A. A.; Kessels, W. M. M. *Chem. Mater.* **2013**, *25*, 1905−1911.
(25) Fan, F.-R.; Liu, D.-Y.; Wu, Y.-F.; Duan, S.; Xie, Z.-X.; Jiang, Z.-Y.; Tian, Z.-Q. *J. Am. Chem. Soc.* **2013**, *130*, 6949−6951.
(26) Peng, Z.; Yang, H. *Nano Today* **2009**, *4*, 143−164.
(27) Xie, S.; Lu, N.; Xie, Z. X.; Wang, J.; Kim, M. J.; Xia, Y. *Angew. Chem., Int. Ed.* **2012**, *51*, 10266−10270.
(28) Xia, X.; Xie, S.; Liu, M.; Peng, H.-C.; Lu, N.; Wang, J.; Kim, M. J.; Xia, Y. *Proc. Natl. Acad. Sci. U.S.A.* **2013**, *110*, 6669−6673.
(29) Choi, S.-I.; Xie, S.; Shao, M.; Odell, J. H.; Lu, N.; Peng, H.-C.; Protsailo, L.; Guerrero, S.; Park, J.; Xia, X.; Wang, J.; Kim, M. J.; Xia, Y. *Nano Lett.* **2013**, *13*, 3420−3425.
(30) Gasteiger, H. A.; Kocha, S. S.; Sompalli, B.; Wagner, F. T. *Appl. Catal., B* **2005**, *56*, 9−35.
(31) Markovic, N. M.; Ross, P. N., Jr. *Surf. Sci. Rep.* **2002**, *45*, 117−229.
(32) Nørskov, J. K.; Rossmeisl, J.; Logadottir, A.; Lindqvist, L. *J. Phys. Chem. B* **2004**, *108*, 17886−17892.
(33) Bligaard, T.; Nørskov, J. K. *Electrochim. Acta* **2007**, *52*, 5512−5516.
(34) Greeley, J.; Mavrikakis, M. *Nat. Mater.* **2004**, *3*, 810−815.
(35) Alayoglu, S.; Nilekar, A. U.; Mavrikakis, M.; Eichhorn, B. *Nat. Mater.* **2008**, *7*, 333−338.
(36) Mavrikakis, M.; Hammer, B.; Nørskov, J. K. *Phys. Rev. Lett.* **2006**, *81*, 2819−2822.
(37) Xie, S.; Choi, S.-I.; Xia, X.; Xia, Y. *Curr. Opin. Chem. Eng.* **2013**, *2*, 142−150.